Contents lists available at ScienceDirect

Journal of Volcanology and Geothermal Research

Seismic monitoring of gas emissions at mud volcanoes: The case of Nirano (northern Italy)

N. Carfagna [a], A. Brindisi [a], E. Paolucci [b], D. Albarello [a,c,*]

[a] Dipartimento di Scienze Fisiche, della Terra e dell'Ambiente, Università degli Studi di Siena, Siena, Italy
[b] Dipartimento di Fisica ed Astronomia, Università degli Studi di Bologna, Bologna, Italy
[c] Consiglio Nazionale delle Ricerche, Istituto di Geologia Ambientale e Geoingegneria, Rome, Italy

ARTICLE INFO

ABSTRACT

Seismic signals generated at the Nirano mud volcanoes in Northern Italy have been monitored by deploying a set of small dimensions seismic arrays of vertical geophones and thee-directional sensors. During two seismic surveys campaigns, seismic signals characterized by sequences of short impulsive signals (lasting 0.1 s–0.2 s) were identified above the background seismic noise. The respective seismic sources have been identified at shallow depths (<30 m) and results sparsely distributed over a wide area. Estimated propagation velocities and polarization analysis indicate that detected pulses also include a significant S waves contribution. These findings have been interpreted as the effect of a stick-slip mechanism due to the interaction between exsolved gas bubbles, mud plugs and the vent walls. On the basis of this model, an estimate of the gas outflow was attempted and results in line with independent measurements of CH_4 and CO_2 emissions carried out in the area.

1. Introduction

Mud volcanoes are the surface expression of overpressured fluid-rich sediments trapped at depth and subject to rapid diagenetic processes (Kopf, 2002). Favoured by the presence of fractures and fault systems, these fluids reach the surface in the form of mud breccia or diapiric mélange, saline water and hydrocarbons, accompanied by large amounts of gases, especially CH_4 and CO_2 (Accaino et al., 2007; Mazzini et al., 2009). The study of mud volcanoes has taken hold for several reasons in the last years: for their implications in energy resource exploration, seismicity, hazard (Martinelli and Panahi, 2003). Moreover, monitoring gas emissions from these structures may be of main interest for evaluating their contribution to the atmospheric budget of greenhouse gases such as methane (Mazzini and Etiope, 2017). However, estimating this contribution is not an easy task. Most of major mud volcanoes are located off-shore in close proximity of convergent plate margins, which prevents a direct outflow estimate. Moreover, also in the case of in-land mud volcanoes, the out-flow phenomena are almost never clustered at the surface, especially the gases emissions, instead they are often widespread in minor vents and mud pools which may be located around main cones (Oppo, 2011). This is the effect of the complex dynamics of the surface outflow, which can be found at several

kilometers away from the main deep reservoir (Thrasher et al., 1996). Recently, some efforts have been devoted to use seismic measurements as a proxy for monitoring gas outflow at mud volcanoes or other vents located at the surface (Albarello et al., 2012; Antunes et al., 2022; La Rocca et al., 2023). Findings from these pioneering studies suggest that cold and hot volcanism share similar phenomenologies. As an example, 'drumbeat' signals, generally associated to degassing activity have been identified in both magmatic volcanic systems (Iverson et al., 2006; Kendrick et al., 2014; Lin, 2017) and mud volcanic contexts (Lupi et al., 2016; Giovani et al., 2017; Antunes et al., 2022; La Rocca et al., 2023). To gain a further insight about the possibility to monitor degassing activity by seismic measurements, a detailed survey has been performed at the *Salse di Nirano* located about 40 km west of Bologna, northern Italy, one of the most known in-land mud volcanoes in Italy (Martinelli and Judd, 2004).

In this area new seismic surveys have been performed by considering a different monitoring setting with aim of providing a more detailed characterization of seismic signals possibly related to the degassing activity.

---

* Corresponding author at: Dipartimento di Scienze Fisiche, della Terra e dell'Ambiente, Università degli Studi di Siena, Siena, Italy.
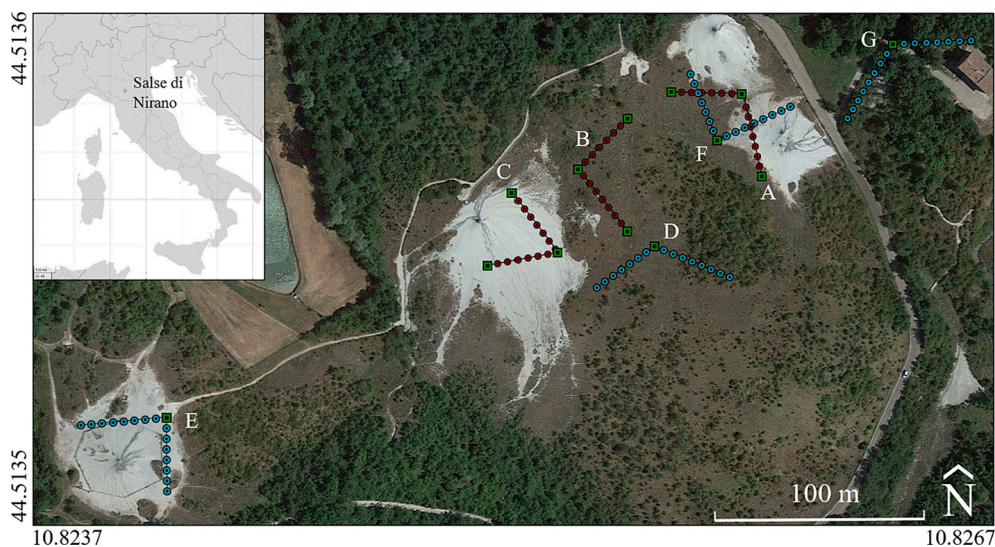 *E-mail address:* dario.albarello@unisi.it (D. Albarello).

Fig. 1. Google Earth satellite image of the Nirano mud volcanoes with seismic instruments used for the surveys. Red and blue dots represent the seismic arrays deployed respectively in 2021 (A, B, C) and 2023 (D, E, F, G). Green squares, in correspondence of the corner geophones of the arrays, represent the locations of the three-components sensors. (For interpretation of the references to colour in this figure legend, the reader is referred to the web version of this article.)

2. The Salse di Nirano site

Existence of mud volcanic phenomenology in the study area is known by centuries, and it is classified as Natural Reserve since 1982.

The area is located within the Apenninic thrust-belt in correspondence of a gently folded formation of relatively rigid Plio-Pleistocenic transgressive clays of marine origin ('*Argille Azzurre*' formation) including occasional sandy lenses. Below a thin (tens of cm) coverage of
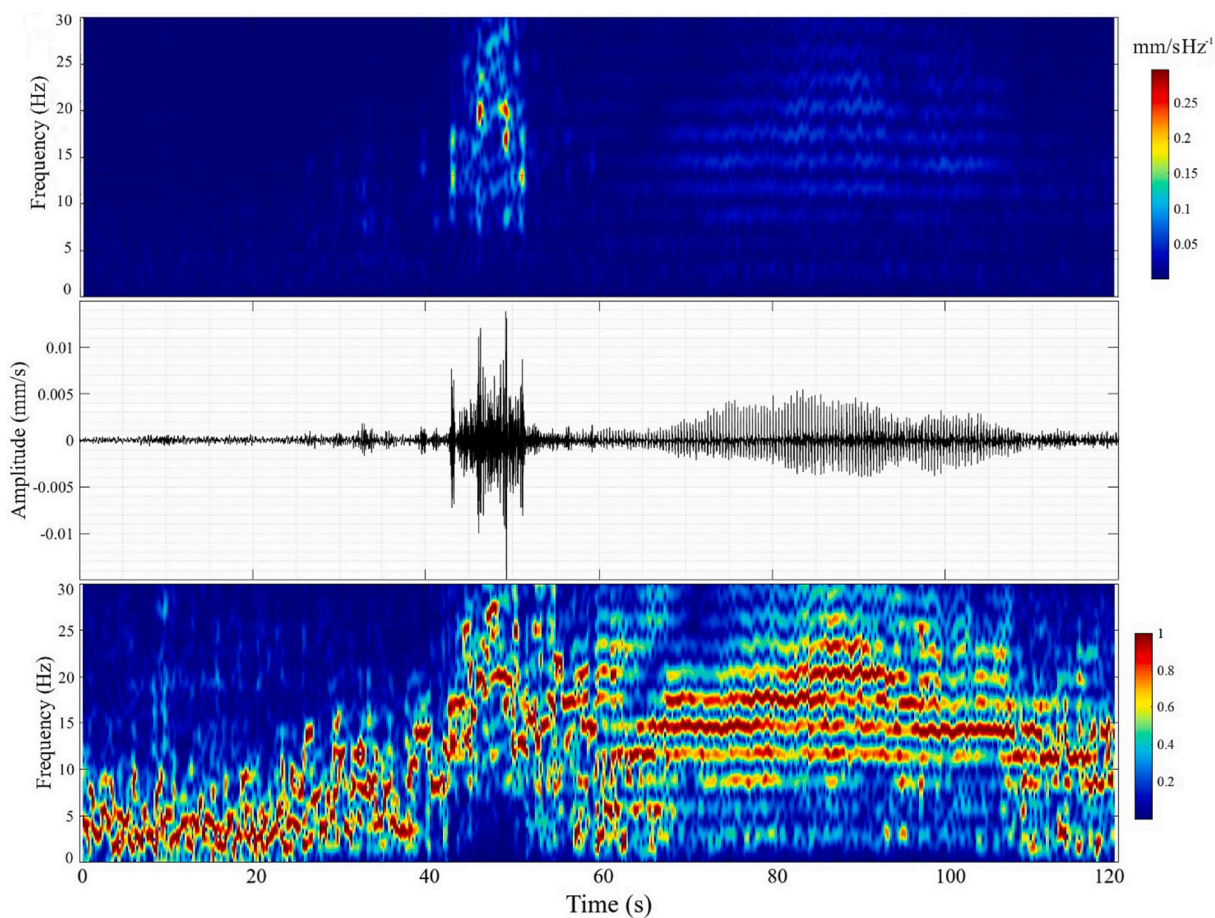

Fig. 2. Time and spectral organization of the seismic signal recorded at a vertical geophone of array A (Fig.1). In the middle, the time series relative to records. In the upper part, the corresponding spectrogram considering a time window of 1 s is reported. In the bottom, to better illustrate how the spectral shape changes during the different phases, spectral amplitudes in each window have been normalized to the respective maximum.
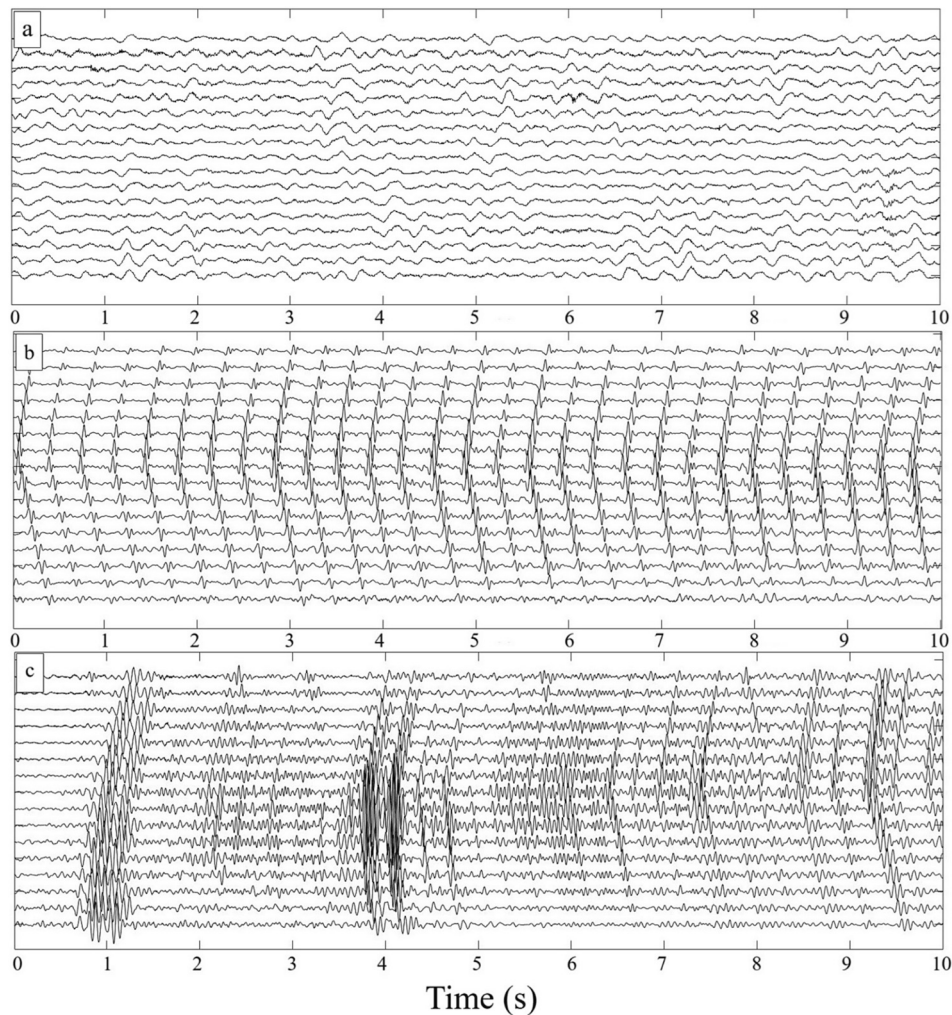
Fig. 3. Typical signals recorded at the vertical geophones of array A (Fig. 1) in at 10s time windows during the quiescent phase (a), and drumbeats characterized by regularly (b) and irregularly (c) sequence of pulses.

muds expelled by the main vents and continuously washed out by meteoric events, the Plio-Pleistocenic bedrock extends down to 50–100 m of depth (Nespoli et al., 2023) and is possibly dissected by buried faults connecting the surface to a deep-seated reservoir (Bonini, 2008, 2009; Lupi et al., 2016). In its central area there are four main volcanic cones at the bottom of an oval depression within a hilly landscape, close to small pools called 'salse'. The largest mud cones reach a height of about 3 m and are all aligned along ENE-WSW direction (Fig. 1). Beyond these main vents, a number of small dimension conduits also exist, which are smeared out in the whole area and show irregular emission activity. Most vents correspond to pools filled by low viscosity mud showing persistent intensity bubbling activity. Temporary dry vents also exist in the area. The conduits relative to these vents may reach depths of tens of meters within the bedrock formation as revealed by geoelectric measurements (Accaino et al., 2007; Lupi et al., 2016; Oppo, 2011) and direct probing (Martinelli G., pers.comm.).

The mud outflowing at the vents and filling the pools is characterized by a viscosity of few mPa s, (slightly larger than that of water) which exhibits a visco-plastic rheology with a flow threshold of the order of few Pa. (Macini and Mesini, 2017).

Gravimetric surveys reveal that the Nirano site is characterized by a significant negative gravity anomaly (Nespoli et al., 2023) and corroborate the hypothesis that the shallow subsoil is characterized by a number of conduits acting as a shallow reservoir between 4 and 20 m depth. In these conduits, low viscosity mud and gas rising deep

structures are trapped and temporarily stored, so that deep fluid ascent is buffered in the shallow subsurface (Giambastiani et al., 2022).

Active and passive surface seismic surveys carried out in the area (Antunes et al., 2022; Brindisi et al., 2023) indicate a rather homogeneous seismic configuration of the shallow subsoil in the study area. Average Vp values have been estimated by of the order 220 m/s, while the average Vs value is of the order of 150 m/s down to a depth of 20 m, where the Vs value apparently increases to about 400 m/s. However, average Horizontal to Vertical Spectral Ratios (HVSR) of ambient vibrations examined by Brindisi et al. (2023) do not show any significant amplitude peak, which indicates the lack of significant 1D seismic resonance phenomena and corresponding site effects.

Geochemical investigations (Oppo, 2011; Sciarra et al., 2019) suggest that gas outflow is not concentrated at the main cones, but it is distributed in a larger area elongated ENE-WSW. More specifically, the NMV northeastern sector has been recently identified as the most active one in terms of gases concentration and flux, even if the general degassing budget linked to the study area is relative low respect to other mud volcanoes in Italy (especially for methane). As an example, Sciarra et al. (2019) measured average CH_4 and CO_2 flux equal to 221 mg m^{-2} d^{-1} and CO_2 18 g m^{-2} d^{-1} respectively. By taking into account respective densities, the overall average volumetric gas outflow results of the order of $9.0\ 10^{-3}$ m^3 d^{-1} m^{-2}.
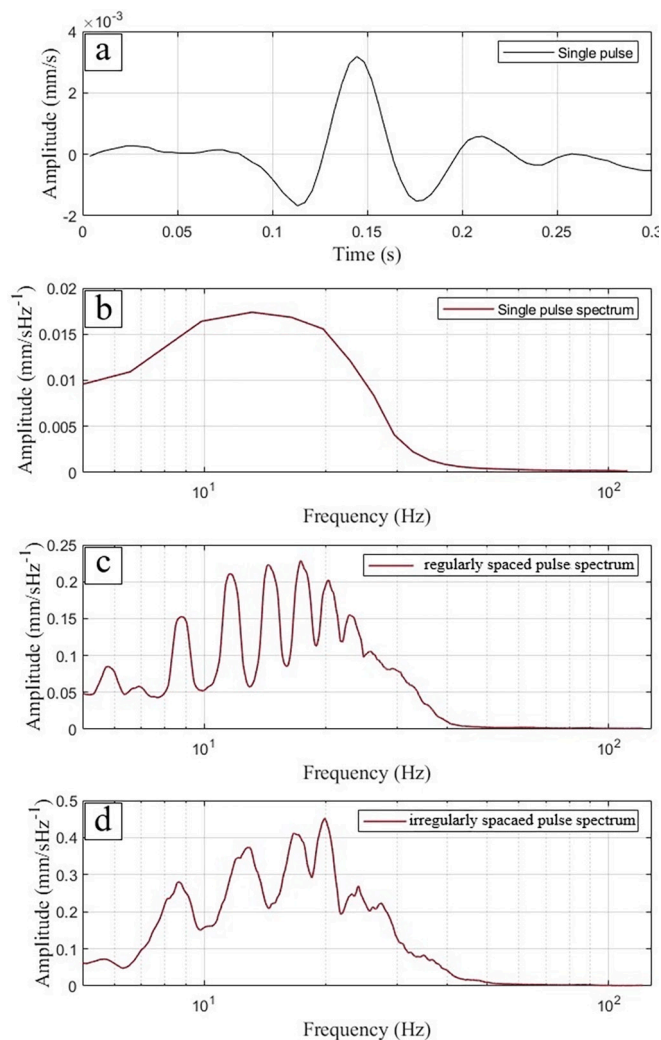
Fig. 4. Comparison among the spectral shape of a single pulse in the drumbeat (*a*, *b*) and the overall spectra relative to two drumbeat sequences in Fig. 2, relative respectively to regularly (*c*) and irregularly (*d*) spaced pulse sequences.

3. The seismic survey

Two seismic surveys campaigns were conducted respectively on 23 April 2021 and about two years later on 12–13 July 2023, using small-scale L-shaped seismic arrays composed of two orthogonal branches of 8 velocimeters each with an interstation distance of 5 m, and three 3-directional velocimeters placed at the corner geophones of the arrays. Measurements (60 min long) were repeated three times around the central-eastern part of the Nirano area in 2021 and four times across the oval depression which holds the main vents in 2023, for a total of seven asynchronous seismic array surveys and 13 3-direction measurements (overall 420 min measurement). Measurements were carried out using 4.5 HZ vertical geophones and a digital acquisition system BrainSpy™ produced by Moho s.r.l. (https://moho.world/). Single-station acquisitions were performed using three-directional 24-bit digital tomograph Tromino™ produced by Moho s.r.l.. In all the records, the same sampling rate (256 sps) has been adopted.

4. Characterization of the seismic signal

In the preceding studies (Antunes et al., 2022; Brindisi et al., 2023) quiescent and paroxysmic seismic activity phases have been recognized in the Nirano area. An example of the typical signal recorded by the vertical geophones in the arrays in Fig. 1, is reported in Fig. 2. Two distinct activity phases are detected at all the arrays, which are characterized by peculiar spectral patterns.

During quiescent phases (see the first part of the signal in Fig. 2), the seismic signal is characterized by relatively low amplitudes (usually between 1 and 2 10^{-4} mm/s) in the frequency range below 4 Hz. This signal is persistent during the whole registration at all the arrays and could represent the ubiquitous background seismic noise related to ambient vibrations generated by natural (wind, sea waves, etc.) and anthropic (industrial activity, vehicular traffic, etc.) sources (e.g., Bonnefoy-Claudet et al., 2006; Nakata et al., 2019).

During paroxysmic phases, instead, amplitudes sharply increase to values of the order of 0.005–0.02 mm/s. These transient phases ('drumbeats') occur irregularly during the registration and are characterized by a peculiar spectral structure (Fig. 2) dominated by higher frequencies (usually between 10 and 30 Hz) with the presence of subsequent sharp peaks. All drumbeats share the same overall spectral shape, and the main difference only concerns the respective position of spectral peaks, which appear more or less regularly spaced in frequency. The peculiar spectral structure of drumbeats can be interpreted as the effect of a sequence of energy pulses (more or less regularly spaced) each characterized by the same spectral structure (see also Neuberg, 2000). In this situation, the frequency spacing between the spectral peaks corresponds to the inverse of the time spacing between the pulses, while the amplitude of the peaks is modulated by the spectral structure of single pulse (see, e.g., Grami, 2015). The visual inspection of the time series relative to quiescent and paroxysmic phases (Fig. 3) confirms thus view: short energy pulses (0.1–0.2 s of duration) occurs during the paroxysmic phases and are lacking (or less evident) in the quiescent phase (Fig. 3). The interevent time regularly spaced pulses is nearly constant and of the order of 0.3 s. Coherently with the above interpretation, the spectral shape of a single pulses strictly mimics the modulation shape of the global drumbeat spectrum (Fig. 4). It is worth to note that, the shape of the pulses is nearly independent from the respective intensity and the location within the specific sequence.

When all the traces of the same array are jointly considered relative to the sequence of pulses (Fig. 3), the moveout of the pulses suggests that any common source exist.

5. Characterizing drumbeat sources

5.1. Pulse detection

An automatic procedure has been implemented to detect and characterize sources of the pulses that compose the drumbeats. At first, pulses registered by each array must be identified by considering two features: their amplitude with respect to the background noise and the correlation with records obtained at neighbourhood sensors (see Fig. 3 b,c). This is achieved by a two steps procedure.

In the first step, seismic pulses are identified in a single reference geophone in the array. To distinguish the pulse from the background noise the STA/LTA detector (Bormann, 2012) has been considered. In this approach, a running time window of length L is defined for the considered seismic trace. This window is subdivided into three sub-windows of equal duration L/3. The standard deviation of the signal registered in the central window (Small Term Average: STA) is compared with the standard deviation of the signal in the remaining part of the window (Long Term Average: LTA). When the ratio STA/LTA is larger than 2, the signal in the central sub-window (with length L/3) is considered representative of a possible pulse signal emerging from the background. When a single potential pulse is identified at the time τ, the corresponding signal is cross correlated with the signal at the nearest geophone by considering a time shift in the range $\tau \pm \Delta t$. When the maximum of the correlogram is above 0.5, the same pulse is assumed to be recorded in the new geophone and the corresponding time shift identifies the corresponding moveout. Then, the same procedure is replicated by considering the new geophone as the reference one. When

Table 1
Pulses detected by the considered arrays during respective activity. N is the number detected of pulses, date is the time of deployment, Ave IET and Var IET are the average and variance of Inter-Event Times (IET) in seconds. In the last column, the ratio between Var IET and Ave IET is reported.

Array	N	Date	Ave IET (s)	Var IET (s)	Ratio
A	1560	April 2021	2.2	5.2	2.3
B	682	April 2021	5.1	8.3	1.6
C	276	April 2021	12.3	29.0	2.4
D	586	July 2023	5.7	7.5	1.3
E	464	July 2023	7.0	11.0	1.6
F	1348	July 2023	2.5	5.6	2.2
G	631	July 2023	5.4	8.5	1.6

the same pulse is identified at a minimum of 5 geophones, the *i-th* event is identified, and the arrival times τ_{ij} relative to each *j-th* geophone are picked out. Two different choices of L were considered (0.3 and 0.6 s) and Δt was chosen as equal to 0.05 s which corresponds to the maximum delay expected for a pulse moving at phase velocity of 100 m/s. It is worth to note, that this procedure focuses on the most energetic phase of the pulse and no attempt is performed to identify the respective onset.

In this way, a large number of pulses has been automatically identified at the arrays (Table 1). As one can see, different activity rates have been detected by each array. However, almost the same rates have been detected by array A and F which have been deployed at almost the same position: this suggests that the process responsible for detected signal is

nearly stationary. Moreover, one can see that the ratios between variance and average inter event times is in all the cases much larger than 1, which implies a significant time clustering of the detected events.

5.2. Source localization

The moveout observed relative to each pulse is considered to identify the relative source. To this purpose, the approximate procedure proposed by Pujol and Smalley (1990) has been adopted. By assuming that propagation occurs within a uniform half space where signal propagates with a phase velocity V_f, the expected arrival time t_{ij} of the *i-th* pulse at each *j-th* geophone can be computed as:

$$t_{ij} = T_i + \frac{1}{V_f}\sqrt{\left(x_j - X_i\right)^2 + \left(y_j - Y_i\right)^2 + Z_i^2} \tag{1}$$

where $\left(x_j, y_j\right)$ is the position of the *j-th* geophone and (X_i, Y_i, Z_i) are the hypocentral coordinates of the source generating the *i-th* pulse at the origin time T_i. This hyperbolic relationship can be rewritten in the linear form as a function of the geophone coordinates as

$$\left(t_{ij} - T_0\right)^2 = ax_j + by_j + c\left(x_j^2 + y_j^2\right) + d \tag{2}$$
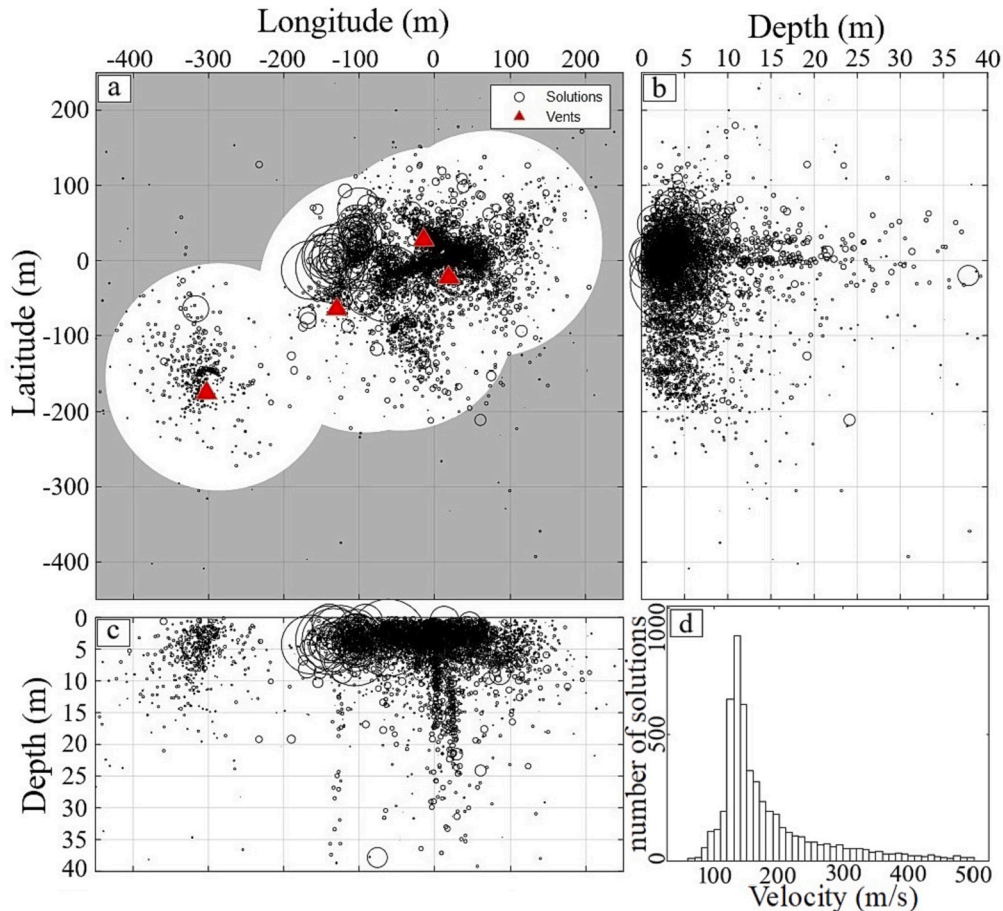
where

Fig. 5. Location of pulse sources and estimated propagation velcoities. Circles indicate the position of the sources and the respective radius is proportional to the estimated radiated energy. Red triangles represent the main vents in the investigated area, while the white area in the panel *a* represents the area with radious of 150 m built around each array where detections of events is considered as reliable; the panels *b* and *c* are two vertical sections of the solutions, in which the vertical scales have been exaggerated; the histogram in panel *d* shows the frequency distribution of propagation velocities releative to the events localized by the automatic procedure. (For interpretation of the references to colour in this figure legend, the reader is referred to the web version of this article.)
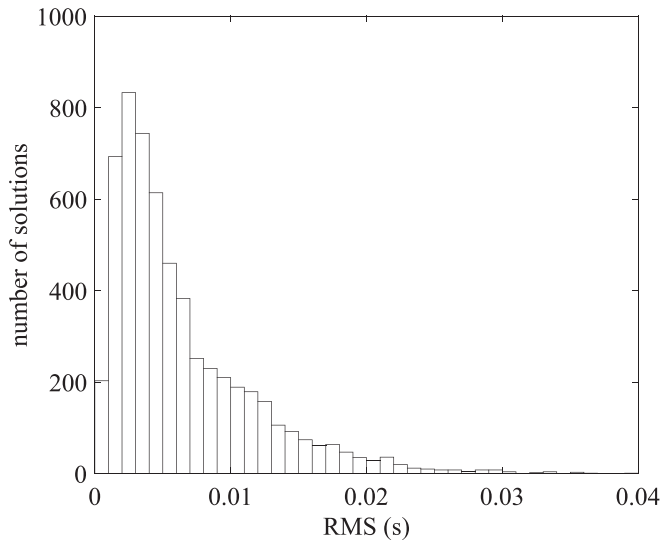
Fig. 6. Frequency distribution of the rms values relative to the hypocentral solutions.

$$a = \left(-\frac{2X_i}{V_f^2}\right); b = \left(-\frac{2Y_i}{V_f^2}\right); c = \frac{1}{V_f^2}; d = \frac{X_i^2 + Y_i^2 + Z_i^2}{V_f^2}$$

Given a tentative guess for T_i (in the range 0–1.0 s), coefficients of eq. [2] (including hypocentral coordinates and phase velocity) are determined by least squares regression to minimize the rms relative to the T_i guess in the form:

$$rms(T_i) = \sqrt{\frac{1}{N_i - 4}\sum_{j=1}^{N_i}\left(\tau_{ij} - t_{ij}\right)^2} \tag{3}$$

The analysis is iterated by considering different guess values of T_i and selecting the one minimizing the respective rms value.

Best fitting hypocentral locations are reported in Fig. 5. As whole, by considering the seven arrays, about 5700 pulses have been identified and located.

The histogram in Fig. 6 reports the frequency distribution of rms values relative to the final hypocentral solutions. Distribution in Fig. 6 has a median of 0.005 s, which is close to the time resolution of the considered records (0.004 s): approximately 80% of the solutions exhibit rms values lower than 0.01 s, i.e., about twice the time resolution. This suggests that the simplified propagation model here considered is effective. Moreover, the rectilinear propagation of the pulses also suggests that no significant P-SV conversion has occurred during propagation and that the shear wave component detected at the arrays should have been generated at the source.

Most of sources are located in the shallower layer (within 10 m from the surface), but deeper events have also been detected down to depths of 20 m and deeper. These relatively deep sources seem to be located in the easternmost and central parts of the considered volume and could suggest the presence of some vertical conduits never detected in the past.

Uncertainty about the hypocentral location depends on the relative position with respect to the array and mainly affects the depths. To have an idea about this uncertainty, 2σ ellipsoids relative to a sample of events is reported in Fig. 7.

To obtain a more realistic image of the detected sources the approach proposed by Peruzza et al. (1991) has been considered. For each detected pulse, 200 random values relative to the regression parameters have been generated by considering a multivariate probability normal distribution with the covariance matrix relative to the least squares best fitting solution. In this way, a probability density function (PDF) is associated to the source responsible for the considered pulse. The PDFs relative to the detected sources are then combined to map the Number of Expected Sources (NES) in the considered area (Fig. 8). The NES distribution confirms the findings obtained from the localization procedure, suggesting that major activity concentrates in the easternmost part of the considered volume, which is in line with findings by Antunes et al. (2022).
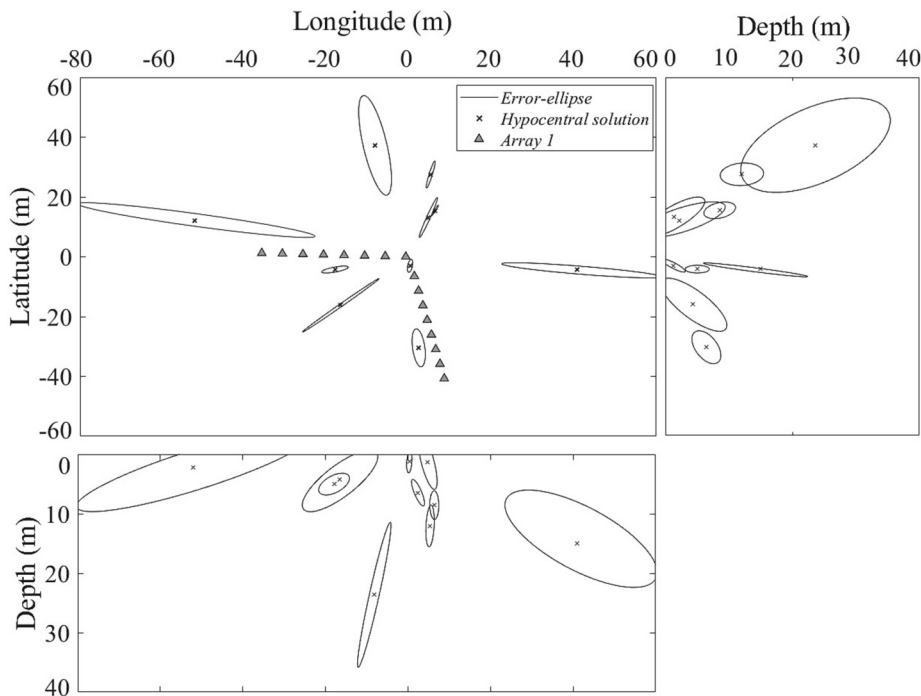

Fig. 7. Uncertatinty affecting hypocentral locations (crosses) of some impulsive events detected by array A. Each ellipsoid represents the 2σ confidence interval relative to respective best fitting solution.
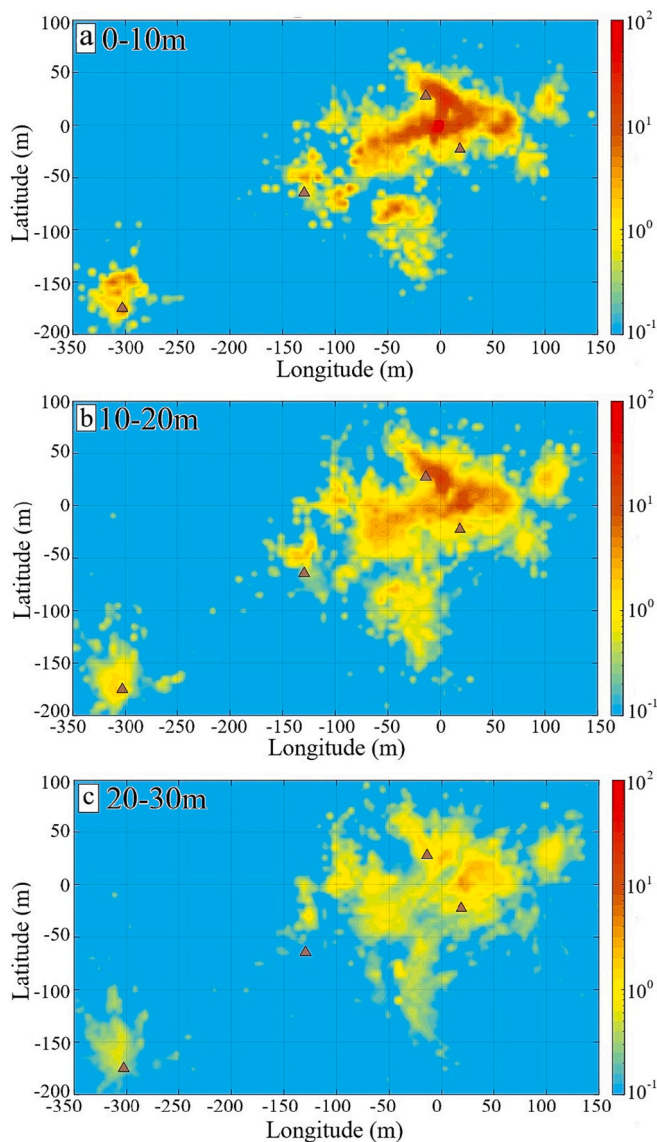
Fig. 8. Distribution of the recorded seismicity expressed by the Number of Expected Sources (NES) variability at different depth ranges: a) 0–10 m; b) 10–20 m; c) 20–30 m. Brown triangles represent the main cones. (For interpretation of the references to colour in this figure legend, the reader is referred to the web version of this article.)

5.3. Pulse characterization

The approach by Pujol and Smalley (1990) described above, also allows the estimation of propagation velocities relative to the detected pulses. The values obtained strongly clusterize around their median value of 155 m/s (Fig. 4d), which is close to the average Vs value in the shallow subsoil obtained by Antunes et al. (2022) and Brindisi et al. (2023). This suggests that most part of energy relative to the detected seismic pulses is mainly carried out by Shear waves. The lack of evident P phases can be also explained by the fact than >80% incidence angles are larger than 70° from the vertical: when observed by vertical geophones (which is the case of the considered arrays), transversal wave motion components are enhanced with respect to the longitudinal ones.

This is also confirmed by the polarization analysis performed by following approach described by Jurkevics (1988) applied to the three-directional registrations of three of the seven arrays. The detected pulses generally show a dominant elliptical polarization on a plane nearly perpendicular to the incidence direction (Fig. 9). Actually, a more

detailed analysis (e.g., Fig. 10) reveals a relatively complex particle motions (possibly due to the small scale lateral heterogeneities present in the shallower subsoil) including a more or less evident longitudinal P waves component.

5.4. Radiated energy

Based on amplitude of registered signals, seismic energy radiated from each source has been estimated by considering attenuation within each array. To this purpose, the approach described in Appendix 1 has been adopted (e.g., Kasahara, 1981). In this analysis, the effect of material damping has been considered only. This last choice is determined by the strong trade-off observed between geometrical spreading coefficient and damping, which does not allow a reliable determination of the respective contributions. Due to the roughness of the model and the fact that short inter-geophonic distances are considered only, a large scattering is expected of the attenuation coefficients. Because of this, a representative attenuation value (0.017) has been considered for the whole area, which corresponds to the median of the distribution in Fig. 11.

Since

$$a = \frac{\pi \nu}{Q V_f} \tag{3}$$

where ν is the frequency of the registered vibration (around 10 Hz), V_f is the phase velocity (150 m/s) and Q is the seismological quality factor (Lay and Wallace, 1995; Chapter 3, Section 3.7), one can see that the medium is characterized by a strong attenuation with a very low-quality factor (about 10). By considering these figures, radiated energies have been estimated for the detected sources (Figs.8). The frequency distribution of radiated energies closely fits a log-normal distribution (Fig. 12) with a median around 0.9 J.

6. An interpretative model

The spread of detected sources over the whole explored area mimics the diffuse gas outflow observed by Sciarra et al. (2019). This suggests that any dynamical relationship could exist between subsoil fluid percolating the sedimentary cover and seismic energy emissions. A physical model of the observed process must be defined to establish any dynamical link between gas outflow and detected seismic signals. Possible analogies between drumbeats at mud volcanoes and magmatic volcanoes have been considered by previous Authors (e.g., Antunes et al., 2022) based on the similarity of observed phenomenology. However, some of the mechanisms proposed to explain drumbeats, including resonance of conduits induced by turbulence phenomena or hydraulic fracturation induced by overpressured fluids (Schick, 1988) do not seem compatible with the low energies associated to the pulses detected at the Nirano mud volcanoes. Resonance phenomena would be unusual due to the disordered and complex conditions of the Nirano context that make it difficult to meet the necessary requirements, while hydraulic fracturing processes require very high pressures that, at such shallow depths (most of located events are above 10 m depth), do not seem very realistic.

The fact that seismic pulses present a significant Shear wave component, contrasts with the hypothesis radiating resonant gas bubbles (Albarello et al., 2012) or expanding fractures due to gas bubbles within soft sediments (Boudreau, 2012). Moreover, some relatively deep events are detected (20 m and more) suggesting that energy is radiated within uprising fluid and this could exclude any seismo-acoustic at the ground-air interface by a ground piston effect (Matoza et al., 2007). More compatible with the drumbeat inner structure of the signal seems to be the presence of any stick-slip mechanism (e.g., Iverson et al. (2006) to explain repeated pulses. Anyway, none of the considered models accounts for the possible rheological behaviour of muds. An alternative
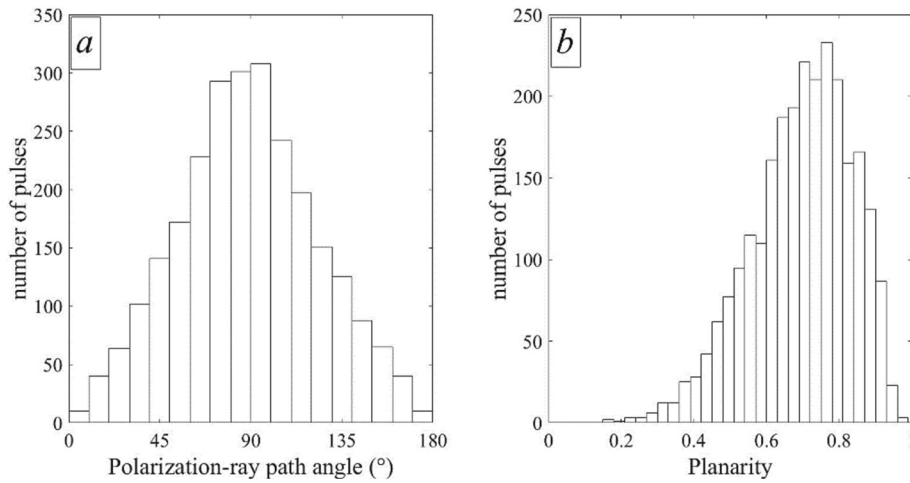
Fig. 9. a) Histogram of the obtained angle formed by the polarization directions and their respective estimated angle of incidence for the events detected by the arrays A,B and C; b) histogram of the elliptical polarization coefficients for the same events.
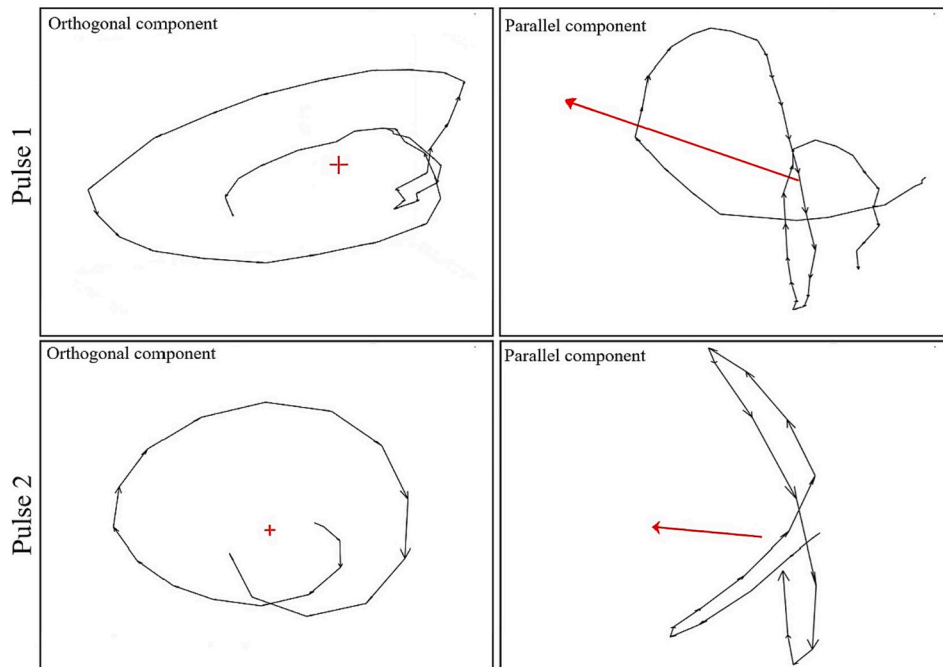

Fig. 10. Examples of particle motion of two different pulses. On the left the particle motion over the plane orthogonal to incidence angle. On the right the particle motion projected on the vertical plane including incidence direction.

model is proposed here below.

To interpret seismic observations at Nirano, we tentatively assume that uprising fluids are constituted by muds including dissolved gas components. During the uprise, the reduction of hydrostatic pressure reduces the solubility of gas and gas bubbles develop by exsolution within the mud (Brown, 1990). This mud/gas mixture reaches the surface through a number of vertical conduits up to a depth of 20-30 m and then percolate within shallow Plio-Pleistocenic rocks through a network of distributed small dimension conduits with relatively rigid walls. This network located just below the surface represents the near surface secondary reservoir of fluids rising from the deep-seated source. Percolation through the conduits is possible because the low viscosity of outflowing mud which has been experimentally determined of the order of few mPa s, slightly larger than that of water (Macini and Mesini, 2017). Moreover, laboratory data also suggest that uprising mud exhibits a visco-plastic rheology with a yield threshold (gel-strength) of the

order of few Pa. The presence of the flow threshold may be at the origin of a static shear stresses resisting the buoyancy forces of the rising gas bubbles pushing upward the mud plug. This threshold may be responsible for the elastic shear load σ_τ active along conduit walls as the effect of a mud plug pushed up by an uprising buoyant gas bubble generated by the exsolution of gas dissolved in the mud. When buoyancy force is below this resisting force, the gas bubble is "frozen" with the conduit. However, gas exsolution may increase the bubble dimension by increasing buoyancy until the resisting force is overcome. This may induce the rapid slip of the mud plug, the release of the elastic energy stored at the conduit boundaries and the consequent emission of seismic energy. Radiated energy can be written in terms of the seismic moment M_0 representative of the slip, the average state of stress σ_a where the seismic pulse has been generated and of the rigidity μ of the conduit (Lay and Wallace, 1995; Chapter 8), in the form
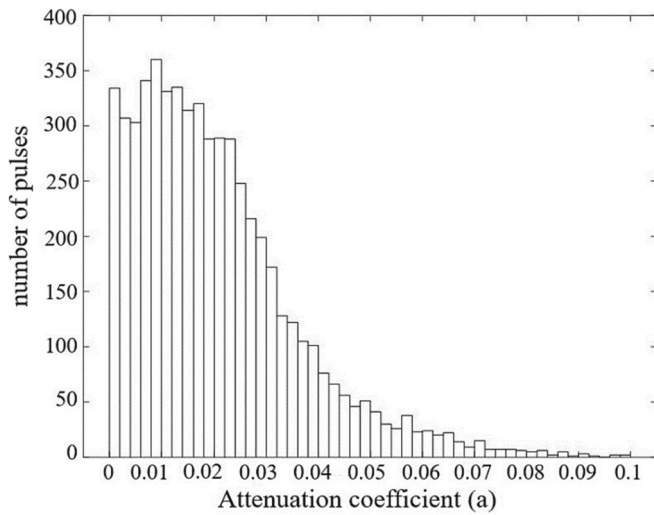
Fig. 11. Frequency distribution of the estimated attenuation coefficients a (eq. [A4]) relative to all considered arrays.

$$E_r \approx \frac{1}{\eta} \sigma_a \frac{M_0}{\mu} = \frac{1}{\eta} \sigma_a u(\pi Dl) \qquad (4)$$

where u is the slip, l is the vertical dimension of the plug, D is the diameter of the cylindrical conduit and η is the seismic efficiency.

The differences among radiated energies depend on the size Dl of the slipping surface, i.e., of the size of the plug. In this view, the log-normal distribution of radiated energies can be explained by the statistical structure of percolation conduits (Kolmogorov, 1941).

The average stress at the depth where pulses origin could be tentatively estimated of the order of the lithostatic load, i.e., $\sigma_a \approx \rho_r g h$, where r_r is the density of rocks surrounding the conduit. By assuming a rock density of the order of 2.10^3 Kg m^{-3}, at a depth of 5 m one has $\sigma_a \approx 10^5$ Pa. Direct observation indicates that the volume of single mud plugs expelled by the main vents are of the order 10^{-4} m^3, the product Dl is expected to be of the order of 10^{-3} m^2. E_r of the order of 1 J on average, one has that u will be of the order of 10^{-2} m for h = 1.

The force F_r resisting the bubble uprise will be

$$F_r = \sigma_\tau \pi Dl = \sigma_\tau \frac{\eta E_r}{u} \qquad (6)$$

While the buoyancy force F$_b$ by the bubble will be

$$F_b = gV(\rho_g - \rho_m) \cong gV\rho_m \qquad (7)$$

where ρ_g and ρ_m are the density of gas and mud respectively, g is gravity acceleration and V is the volume of the gas bubble. When the slip begins, one should have $F_r \approx F_b$ which means

$$\sigma_\tau \frac{\eta E_r}{u} = gV\rho_m \rightarrow V = \sigma_\tau \frac{\eta}{ug\rho_m} E_r \qquad (8)$$

Since $g\rho_m$ is of the order of 10^4 Nm^{-3} and u is of the order of 10^{-2} m, if one assumes again $\eta = 1$ (thermal dissipation is considered as negligible), the volume of gas bubbles responsible for the pulse will be

$$V \approx 10^{-2} E_r \qquad (9)$$

which allows estimating the volume of uprising gas bubbles from radiated seismic energy.

Eq. [9] can be used to estimate gas outflow from radiated seismic energies. In particular, one has that the average gas flow $\overline{\phi}$ (m^{3}d^{-1} m^{-2}) can be computed as

$$\overline{\phi} = \frac{1}{\pi R^2} \frac{24}{7} \sum_{i=1}^{N} V_i \qquad (10)$$

where N is the overall number of pulses detected by the 7 arrays operating for 1 h each and E_i are the corresponding radiated energies. R is the radius of the area where all seismic sources are expected to have been detected (150 m). The estimated outflow results of the order of 8.7 10^{-3} m^{3}d^{-1} m^{-2}.

This average estimate is very close to the one obtained by Sciarra et al. (2019) based on direct outflow measurements. More detailed comparisons relative to lateral variations of the gas outflow estimated by the two approaches cannot provide reliable outcomes. This because gas outflow has been measured at the surface at well localized sites, while seismic pulses have been localized (rather approximately) at some depth: thus no one-to-one correspondence is expected between the sets of measurements. Moreover, data relative to gas outflow were collected between 2015 and 2016, while seismic monitoring has been performed between 2021 and 2023. Since a number of minor gas vents exists whose activity rapidly changes in time, the comparison between the estimates provided by seismic measurements and those by geochemical surveys cannot be compared in detail, but only in terms of average values.

In the model depicted above, the intermittent pulse emission could be explained as follows. When the slug is displaced upward, the upper bound of the gas bubble displaces upward by providing a sudden
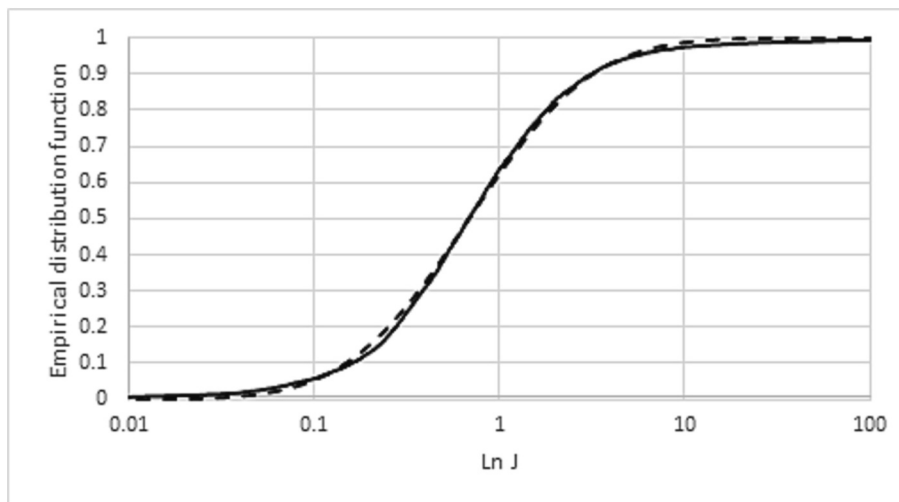

Fig. 12. Comparison between empirical frequency distribution of radiated energy values (dashed line) and the log normal probability distribution with average − 0.16, and standard deviation 0.52 (continuous line).

increase of bubble volume and, as a consequence in an adiabatic situation, the reduction of gas pressure within the bubble. This reduces the pressure exerted on the plug below resisting forces. Until the pressure is restored by gas exsolution (prompted by the pressure reduction within the bubble), the slug uprise stops to start again when the restoration is complete. Moreover, possible transient effects may characterize the mud, including a shear rate dependence of gel strength (e.g., Malkin et al., 2023). This effect may imply a difference between static and dynamic yield stress eventually responsible for a stick-slip behaviour. Clustering of pulses (the drumbeat) could be the expression of different amounts of dissolved gas within uprising muds, where depleted and gas rich muds may alternate.

7. Conclusions

The deployment of small seismic arrays allowed to gain new insights about seismic signals emitted from the Nirano mud volcanoes. With respect to these preceding experiences, this configuration allowed the identification of a large number of weak and short impulsive signals, by putting in evidence their peculiar space and time distributions within the "drumbeats" detected by previous studies (e.g., Antunes et al., 2022; Brindisi et al., 2023). The array configuration and the joint use of three-dimensional measurements allowed the characterization observed pulses. Most of the sources of these pulses are located within 10 m from the surface within a volume of relatively old sedimentary rocks characterized by strong attenuation and possible small-scale heterogeneities. The above sources are sparsely distributed over a wide area without any evidence of possible concentration at the main cones. Some weak evidence also supports the idea that a number of vertical conduits also exist, possibly connecting the volume where the shallow seismic sources are located to the deep-seated reservoir.

This results in line with outcomes of gas outflow measurements (Sciarra et al., 2017, 2019), and it suggests a possible dynamical connection between gas emission and seismic signals. To account for the above pieces of evidence a dynamical model is presented, which also considers the rheological behaviour of muds in the Nirano area. This model allows establishing a quantitative relationship between radiated energies relative to observed pulses and gas outflow. The application of this model to observations showed nearly perfect agreement between estimates provided by seismic observations and measured gas outflow provided by Sciarra et al. (2019) for the Nirano area. This result suggests that seismic observations could represent a useful tool for monitoring gas outflow at mud volcanoes, which could be very effective where direct observation of gas emissions are hampered by environmental conditions such as in the case of off-shore mud volcanoes.

CRediT authorship contribution statement

N. Carfagna: Conceptualization, Methodology, Software, Writing – review & editing. **A. Brindisi:** Data curation, Investigation. **E. Paolucci:** Data curation, Investigation. **D. Albarello:** Conceptualization, Formal analysis, Funding acquisition, Methodology, Supervision, Writing – original draft.

Declaration of Competing Interest

The authors declare that they have no known competing financial interests or personal relationships that could have appeared to influence the work reported in this paper.

Data availability

Data will be made available on request.

Acknowledgments

Appendix 1. Appendix

At a velocimetric sensor, a monochromatic signal with period T_0 and amplitude $\dot{u}_0$ is observed in the form

$$\dot{u}(t) = \dot{u}_0 sin\left(\frac{2\pi t}{T_0}\right) \tag{A1}$$

The average kinetic energy e per unit volume and unit time associated to that signal is

$$\varepsilon = \frac{1}{2}\rho \frac{1}{T_0}\int_0^{T_0} \dot{u}_0^2 sin^2\left(\frac{2\pi t}{T_0}\right)dt = \frac{1}{4}\rho \dot{u}_0^2 \tag{A2}$$

If the signal has a duration t_0 and propagates with a velocity V_f, the energy flow ϕ at the surface (ignoring the effect of surface reflection) and considering that, on overage, kinetic and potential energy are equal, the total energy flow will be

$$\phi = V_f t_0 \varepsilon = \frac{1}{2}V_f t_0 \rho \dot{u}_0^2 \tag{A3}$$

If the signal is observed at a distance d from a point-like source and the material damping is considered, one has

$$\phi(r) = \varepsilon V_f t_0 = \left(\frac{1}{2}\rho \dot{u}_0^2 \, V_f t_0\right)e^{-ad} = \phi_0 e^{-ad} \tag{A4}$$

where a represents the effect of material damping. If the wave train corresponds to a spherical wavefront, the total energy E_r radiated at the source will be

$$E_r = \phi_0 4\pi d^2 \tag{A5}$$

References

Accaino, F., Bratus, A., Conti, S., Fontana, D., Tinivella, U., 2007. Fluid seepage in mud volcanoes of the northern Apennines: an integrated geophysical and geological study. J. Appl. Geophys. 63, 90–101. https://doi.org/10.1016/j.jappgeo.2007.06.002.

Albarello, D., Palo, M., Martinelli, G., 2012. Monitoring methane emission of mud volcanoes by seismic tremor measurements: a pilot study. NHESS 12, 3617–3629. https://doi.org/10.5194/nhess-12-3617-2012.

Antunes, V., Planes, T.O., Panzera, F., D'Amico, S., Mazzini, A., Sciarra, A., Lupi, M., 2022. Insights into the dynamics of the Nirano Mud Volcano through seismic characterization of drumbeat signals and V/H analysis. J. Volcanol. Geotherm. Res. 431 https://doi.org/10.1016/j.jvolgeores.2022.107619.

Bonini, M., 2008. Elliptical mud volcano caldera as stress indicator in an active compressional setting (Nirano, Pede-Apennine margin, northern Italy). Geology 36, 131–134. https://doi.org/10.1130/G24158A.1.

Bonini, M., 2009. Mud volcano eruptions and earthquakes in the Northern Apennines and Sicily, Italy. Tectonophys. 474, 723–735. https://doi.org/10.1016/j.tecto.2009.05.018.

Bonnefoy-Claudet, S., Cotton, F., Bard, P.Y., 2006. The nature of noise wavefield and its applications for site effects studies: a literature review. Earth Sci. Rev. 79, 205–227.

Bormann, P., 2012. New Manual of Seismological Observatory Practice (NMSOP-2), IASPEI. GFZ German Research Centre for Geoscience, Potsdam. https://doi.org/10.2312/GFZ.NMSOP-2.

Boudreau, B.P., 2012. The physics of bubbles in surficial, soft cohesive sediments. Mar. Petr.Geol. 38, 1–18. https://doi.org/10.1016/j.marpetgeo.2012.07.002.

Brindisi, A., Carfagna, N., Paolucci, E., Albarello, D., 2023. Fine structure of seismic emissions from Nirano mud volcanoes (northern Apennines, Italy): a phenomenological study. In press on Bull. Geophys. Oceanogr. https://doi.org/10.4430/bgo00437.

Brown, K.M., 1990. The nature and hydrogeologic significance of mud diapirs and diatremes for accretionary systems. J.Geophys. Res. 95, 8969–8982.

Giambastiani, B.M.S., Antonellini, M., Nespoli, M., Bacchetti, M., Calafato, A., Conventi, M., Dadomo, A., Martinelli, G., Morena, M., Venturoli, S., Piombo, A., 2022. Mud flow dynamics at gas seeps – Nirano *Salse*, Italy. Environ. Earth Sci. 81, 480 (2022). https://doi.org/10.1007/s12665-022-10615-2.

Giovani, L., Vallocchia, M., Antunes, V., Lupi, M., Oberman, A., Mazzini, A., Moretti, M., 2017. Esperimento di sismica passiva per lo studio di dettaglio dei vulcani di fango nella Riserva Naturale Regionale delle Salse di Nirano (Modena). Technical Report, INGV, p. 382.

Grami, A., 2015. Introduction to Digital Communications. Academic Press, 604 pp., ISBN: 9780124076822.

Iverson, R.M., Dzurisin, D., Gardner, C.A., Gerlach, T.M., LaHusen, R.G., Lisowski, M., Vallance, J., 2006. Dynamics of seismogenic volcanic extrusion at Mount St Helens in 2004-05. Nature 444, 439–443. https://doi.org/10.1038/nature05322.

Jurkevics, A., 1988. Polarization analysis of three-component array data. Bull.Seism.Soc. Am. 78 (5), 1725–1743.

Kasahara, K., 1981. Earthquake Mechanics. Cambridge University Press, 284 p.

Kendrick, J.E., Lavallée, Y., Hirose, T., Di Toro, G., Hornby, A., De Angelis, S., Dingwell, D., 2014. Volcanic drumbeat seismicity caused by stick-slip motion and magmatic frictional melting. Nat.Geosci. 7, 438–442. https://doi.org/10.1038/NGEO2146.

Kolmogorov, A., 1941. The Local Structure of Turbulence in Incompressible Viscous Fluid for very large Reynolds Number. Doklady Akademii Nauk SSSR 30, 301–304.

Kopf, A.J., 2002. Significance of mud volcanism. Rev. Geophys. 40 (2), 52.

La Rocca, M., Galluzzo, D., Nardone, L., Gaudiosi, G., Di Luccio, F., 2023. Hydrothermal seismic tremor in a wide frequency band: the nonvolcanic CO2 degassing site of Mefite d'Ansanto, Italy. Bull.Seism.Soc.Am 113, 1102–1114. https://doi.org/10.1785/0120220243.

Lay, T., Wallace, T., 1995. Modern Global Seismology. Academic Press, Inc., Cambridge, MA.

Lin, C.-H., 2017. Dynamic triggering of volcano drumbeat-like seismicity at the Tatun volcano group in Taiwan. Geophys.J.Int. 210, 354–359. https://doi.org/10.1093/gji/ggx172.

Lupi, M., Ricci, B.S., Kenkel, J., Ricci, T., Fuchs, F., Miller, S.A., Kemna, A., 2016. Subsurface fluid distribution and possible seismic precursory signal at the Salse di Nirano mud volcanic field, Italy. Geophys.J.Int. 204, 907–917. https://doi.org/10.1093/gji/ggv454.

Macini, P., Mesini, E., 2017. Indagini sperimentali sulle caratteristiche reologiche di alcuni fanghi emergenti dalle Salse di Nirano. 148. Atti della Società dei Naturalisti e Matematici di Modena – Supplemento.

Malkin, A.Y., Darkach, S.R., Kulichikhin, V.G., 2023. Rheology of gels and yielding liquids. Gels 9 (9), 715. https://doi.org/10.3390/gels9090715, 2023.

Martinelli, G., Judd, A., 2004. Mud volcanoes of Italy. Geol.J. 39, 49–61.

Martinelli, G., Panahi, B., 2003. Mud Volcanoes, Geodynamics and Seismicity, vol. 51. IOS Press. NATO Science Series,.

Matoza, R., Hedlin, M., Garcés, M., 2007. An infrasound array study of Mount St. Helens. J. Volcanol. Geotherm. Res. 160, 249–262.

Mazzini, A., Etiope, G., 2017. Mud volcanism: an updated review. Earth Sci. Rev. 168, 81–112. https://doi.org/10.1016/j.earscirev.2017.03.001.

Mazzini, A., Nermoen, A., Krotkiewski, M., Podladchikov, Y., Planke, S., Svensen, H., 2009. Strike-slip faulting as a trigger mechanism for overpressure release through piercement structures. Implications for the Lusi mud volcano, Indonesia. Mar.Pet. 26, 1751–1765. https://doi.org/10.1016/j.marpetgeo.2009.05.003.

Nakata, N., Gualtieri, L., Fichtner, A., 2019. Seismic Ambient Noise. Cambridge University Press. https://doi.org/10.1017/9781108264808.

Nespoli, M., Antonellini, M., Albarello, D., Lupi, M., Cenni, N., Rivalta, E., Piombo, A., 2023. From Gravity data a novel interpretation for the dynamics of mud volcanism at the Nirano Salse. Gephys.Res.Lett. 50 (20) https://doi.org/10.1029/2023GL103505 e2023GL103505.

Neuberg, J., 2000. Characteristics and causes of shallow seismicity in andesite volcanoes. Philos. Trans. R. Soc. Series A 358, 1533–1546.

Oppo, D., 2011. Studio dei vulcani di fango per la definizione della migrazione dei fluidi profondi. PhD thesis. University of Bologna, Department of Earth and Geological-Environmental Sciences.

Peruzza, L., Rebez, A., Slejko, D., Padoan, G., 1991. Weighted uncertainties used to detect seismogenic structures. Boll.Geofis.Teor.Appl. 33 (129), 25–45.

Pujol, J., Smalley, R., 1990. A preliminary earthquake location method based on a hyperbolic approximation to travel times. Bull.Seism.Soc.Am. 80 (6), 1629–1642.

Schick, R., 1988. Volcanic tremor-source mechanisms and correlation with eruptive activity. Nat. Hazards 1, 125–144.

Sciarra, A., Cantucci, B., Conventi, M., Ricci, T., 2017. Caratterizzazione geochimica e monitoraggio dei flussi e delle componenti gassose nella Riserva delle Salse di Nirano. 148. Atti della Società dei Naturalisti e Matematici di Modena - Supplemento.

Sciarra, A., Cantucci, B., Ricci, T., Tamonaga, Y., Mazzini, A., 2019. Geochemical characterization of the Nirano mud volcano, Italy. Appl. Geochem. 102, 77–87. https://doi.org/10.1016/j.apgeochem.2019.01.006.

Thrasher, J., Fleet, A., Hay, S., Hovland, M., Düppenbecker, S., 1996. Understanding geology as the key to using seepage in exploration: the spectrum of seepage styles. In: Hydrocarbon Migration and its Near-Surface Expression. AAPG, 66, pp. 223–241. https://doi.org/10.1306/m66606c17.